Article

Cu(II) Coordination Polymers Containing Mixed Ligands with Different Flexibility: Structural Diversity and Iodine Adsorption

Shu-Yu Lin , Yi-Lin Shen , Wei-Hao Chen , Manivannan Govindaraj * , Jhy-Der Chen *

Posted Date: 5 December 2023

doi: 10.20944/preprints202312.0220.v1

Keywords: coordination polymer; crystal structure analysis; tricarboxylate; coordination mode

Preprints (www.preprints.org) | NOT PEER-REVIEWED | Posted: 5 December 2023 doi:10.20944/preprints202312.0220.v1

Article

Cu(II) Coordination Polymers Containing Mixed Ligands with Different Flexibility: Structural Diversity and Iodine Adsorption

Shu-Yu Lin [1], Yi-Lin Shen [1], Wei-Hao Chen[1], Manivannan Govindaraj [2,*] and Jhy-Der Chen [1,*]

[1] Department of Chemistry, Chung Yuan Christian University, Chung Li, Taoyuan City 320, Taiwan; kikimy123kikimy123@yahoo.com.tw (S.-Y.L.); lin740240@gmail.com (Y.-L.S.); a88q1127@gmail.com (W.-H.C.)
[2] Department of Chemistry, Periyar Maniammai Institute of Science & Technology (Deemed to be University), Vallam, Thanjavur, 613 403, Tamil Nadu, India;
* Correspondence: manivannang@pmu.edu (M.G); jdchen@cycu.edu.tw (J.-D.C.); Tel.: +886-3-265-3351 (J.-D.C.)

Abstract: Reactions of *N,N′*-bis(3-methylpyridyl)oxalamide (**L**^{1}), *N,N′*-bis(3-methylpyridyl)adipoamide (**L**^{2}) and *N,N′*-bis(3-methylpyridyl)sebacoamide (**L**^{3}) with tricarboxylic acids and Cu(II) salts afforded $\{[\mathrm{Cu}(\mathbf{L}^1)(1,3,5\text{-HBTC})]\cdot \mathrm{H_2O}\}_n$ ($1,3,5\text{-H}_3\text{BTC}$ = 1,3,5-benzenetricarboxylic acid), **1**, $\{[\mathrm{Cu}_{1.5}(\mathbf{L}^2)_{1.5}(1,3,5\text{-BTC})(\mathrm{H_2O})_2]\cdot 6.5\mathrm{H_2O}\}_n$, **2**, $[\mathrm{Cu}(\mathbf{L}^2)_{0.5}(1,3,5\text{-HBTB})]_n$ ($1,3,5\text{-H}_3\text{BTB}$ = 1,3,5-tri(4-carboxyphenyl)benzene), **3**, $[\mathrm{Cu}_4(\mathbf{L}^3)(\mathrm{OH})_2(1,3,5\text{-BTC})_2]_n$, **4**, $\{[\mathrm{Cu}_3(\mathbf{L}^3)_2(1,3,5\text{-BTB})_2]\cdot 2.5\mathrm{MeOH}\cdot 2\mathrm{H_2O}\}_n$, **5**, and $\{[\mathrm{Cu}_3(\mathbf{L}^3)_2(1,3,5\text{-BTB})_2]\cdot \mathrm{DMF}\cdot 2\mathrm{H_2O}\}_n$, **6**, which have been structurally characterized by using single crystal X-ray crystallography. Complexes **1** – **4** form a 2D layer with the $\{4^4.6^2\}$-**sql** topology, a 2D layer with the $(4.6^2)_2(4^2.6^2.8^2)$-**bex** topology, a 3-fold interpenetrated 3D net with the $(4^{12}\cdot 6^3)$-**pcu** topology and a 3D framework with the $(4^{10}\cdot 6^{32}\cdot 8^3)(4^2\cdot 6)_2(4^3\cdot 6^3)$ topology, respectively, whereas **5** and **6** are 3D frameworks with the $(6^3)_2(6^4\cdot 8^2)(6^8\cdot 8^5\cdot 10^2)$ topology. Complex **5** shows a better iodine-adsorption factor of 290.0 mg g^{-1} at 60 ^{o}C for 360 minutes than the other ones, revealing that the flexibility of the spacer ligand governs the structural diversity and the adsorption capacity.

Keywords: coordination polymer; crystal structure analysis; tricarboxylate; coordination mode

1. Introduction

Coordination polymers (CPs) have shown crucial applications in many different areas due to their diverse structures and variable functions [1–7]. CPs can be constructed by the coordination of the designable spacer ligands to the metal ions, and through the self-assembly process, one- (1D), two- (2D) or three-dimensional (3D) network structures can be prepared.

The $-(\mathrm{CH_2})_n-$ group of the bis-pyridyl-bis-amide (bpba) possesses suitable flexibility that may adopt the coordination environment of different metal ions, whereas the two amide groups play important roles as abundant potential hydrogen bond sites, affording CPs with remarkable topologies [8]. On the other hand, polycarboxylate ligands that show distinct coordination modes involving chelating and bridging are also important in the organization of CPs in a mixed system [9]. Benzene-1,3,5-tricarboxylic acid ($1,3,5\text{-H}_3\text{BTC}$) is a planar molecule with C_3-symmetry that may give anions of the types, BTC^{3-} and HBTC^{2-}, and intriguing structural types have been found in the bpba-based CPs supported by these anions [10–12]. Extension of $1,3,5\text{-H}_3\text{BTC}$ to the larger 1,3,5-tri(4-carboxyphenyl)benzene ($1,3,5\text{-H}_3\text{BTB}$) may thus afford CPs with different structural topology.

We are dedicated to illuminate the factors that may direct the structural diversity and govern the adsorption property of the flexible bpba-based CPs by exploring the variations in ligand conformation and coordination mode of the spacer ligands. In this study, flexible *N,N′*-bis(3-pyridylmethyl)oxalamide (L^1), *N,N′*-bis(3-methylpyridyl)adipoamide (L^2) and *N,N′*-bis(3-methylpyridyl)sebacoamide (L^3), Figure 1, were reacted with the Cu(II) metal salts and the tricarboxylic acids, 1,3,5-H_3BTC, and 1,3,5-H_3BTB, Figure 2, to yield {[Cu(L^1)(1,3,5-HBTC)]·H_2O}$_n$ (1,3,5-H_3BTC = 1,3,5- benzenetricarboxylic acid), 1, {[$Cu_{1.5}$(L^2)$_{1.5}$(1,3,5-BTC)(H_2O)$_2$]·6.5H_2O}$_n$, 2, [Cu(L^2)$_{0.5}$(1,3,5-HBTB)]$_n$ (1,3,5-H_3BTB = 1,3,5-tri(4-carboxyphenyl)benzene), 3, [Cu_4(L^3)(OH)$_2$(1,3,5-BTC)$_2$]$_n$, 4, {[Cu_3(L^3)$_2$(1,3,5-BTB)$_2$]·2.5MeOH·2H_2O}$_n$, 5, {[Cu_3(L^3)$_2$(1,3,5-BTB)$_2$]·DMF·2H_2O}$_n$, 6. The synthesis and structures of 1 – 6 as well as their iodine adsorptions form the subject of this report.

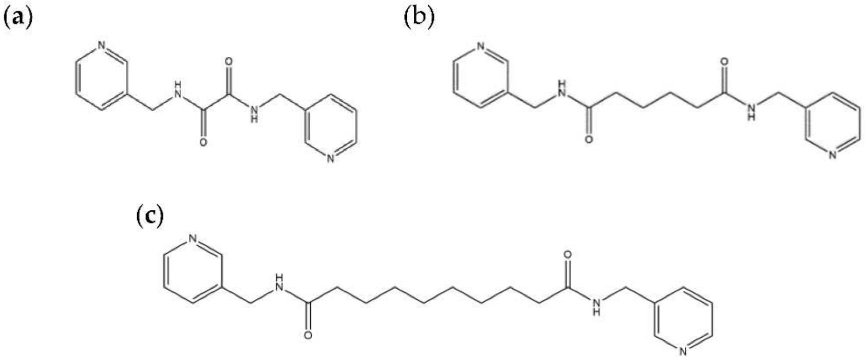

Figure 1. Structures of (**a**) **L**^{1}, (**b**) **L**^{2} and (**c**) **L**^{3}.

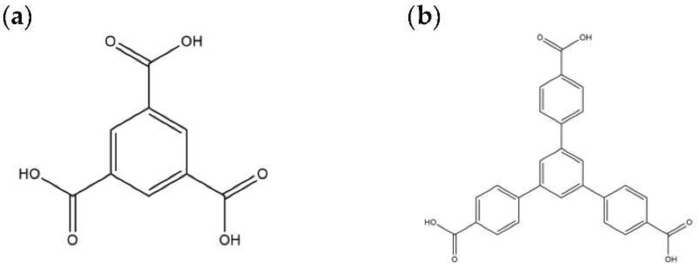

Figure 2. Structures of (a) 1,3,5-H_3BTC and (b) 1,3,5-H_3BTB.

2. Results and Discussion

2.1. Structure of **1**

A single-crystal X-ray diffraction analysis shows that complex **1** crystallizes in the triclinic space group $P\bar{1}$. There are one Cu(II) cation, one **L**^{1} ligand, one 1,3,5-HBTC^{2-} ligand and one cocrystallized water molecule in the asymmetric unit. The Cu(II) atom is coordinated by two nitrogen atoms from **L**^{1} ligands [Cu-N = 2.001(3) - 2.007(3) Å] and three oxygen atoms from three 1,3,5-HBTC^{2-} ligands [Cu-O = 1.966(3) - 2.237(3) Å], resulting in a trigonal bipyramidal geometry, and a dicopper unit bridged by the 1,3,5-HBTC^{2-} ligands, Figure 3a. The Cu(II) ions are linked together by 1,3,5-HBTC^{2-} and **L**^{1} ligands to afford a 2D structure. If the 1,3,5-HBTC^{2-} ligands are considered as 3-connected nodes and the Cu(II) ions as 5-connected nodes, the structure of **1** can be simplified as 3,5-connected binodal 2D net with the ($4^2·6^7·8$)($4^2·6$)-3,5L2 topology (standard representation), Figure 3b.determined by using TopoPro program [13]. If the dinuclear Cu(II) units are defined as 4-connected nodes, the structure can be simplified as a 4-connected net with the ($4^4·6^2$)-**sql** topology (cluster representation), Figure 3c.

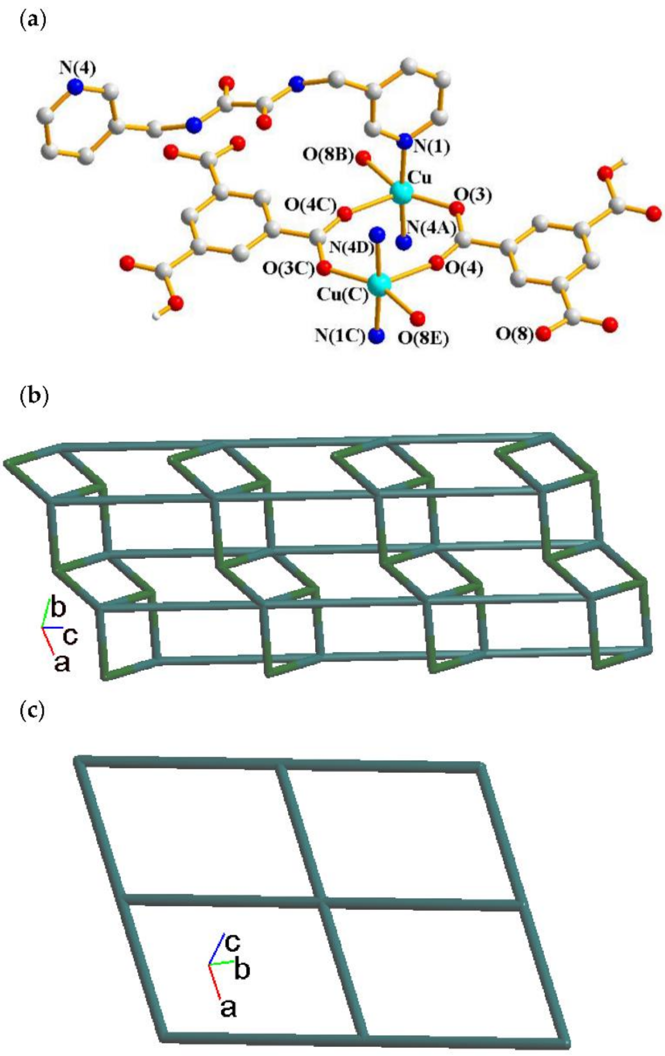

Figure 3. (a) Coordination environments of the Cu(II) ion in **1**. Symmetry transformations used to generate equivalent atoms: (A) x-1, y-1, z -1; (B) x + 1, y, z; (C) -x + 1, -y + 2, -z + 1; (D) -x + 2, -y + 3, -z + 2; (E) -x, -y + 2, -z + 1. (b) A drawing showing the 2D net with the $(4^2{\cdot}6^7{\cdot}8)(4^2{\cdot}6)$-3,5L2 topology. (c) A drawing showing the 2D net with the $(4^4{\cdot}6^2)$-**sql** topology.

2.2. Structure of **2**

Crystals of complex **2** conform to the triclinic space group $P\bar{1}$ and each asymmetric unit consists of two Cu(II) cations, one and a half of an **L**^{2} ligands, one 1,3,5-BTC^{3-} ligand, two coordinated water and six and a half of a cocrystallized water molecules. The Cu(1) and Cu(2) metal centers are four- and five-coordinated, respectively, Figure 4a. While the Cu(1) atom is coordinated by two nitrogen atoms from the **L**^{2} ligand [Cu-N = 2.051(2) Å] and two oxygen atoms from two 1,3,5-BTC^{3-} ligands [Cu-O = 1.960(2) Å], resulting in a distorted square geometry, the Cu(2) atom is coordinated by two nitrogen atoms from two **L**^{2} ligands [Cu-N = 2.000(3) - 2.006(3) Å], one oxygen atom from the 1,3,5-BTC^{3-} ligand [Cu-O = 1.978(2) Å] and two oxygen atoms from two coordinated water molecules [Cu-O = 2.023(2) – 2.200(2) Å], giving a square pyramidal geometry. The Cu(II) ions are linked together by the 1,3,5-BTC^{3-} and **L**^{2} ligands to afford a 2D layer. If the Cu(1) cations are defined as 4-connected nodes and Cu(2) cations as 3-connected nodes, the structure can be simplified as a 3,4-connected 2D net with the $(4.6^2)_2(4^2.6^2.8^2)$-**bex** topology, Figure 4b.

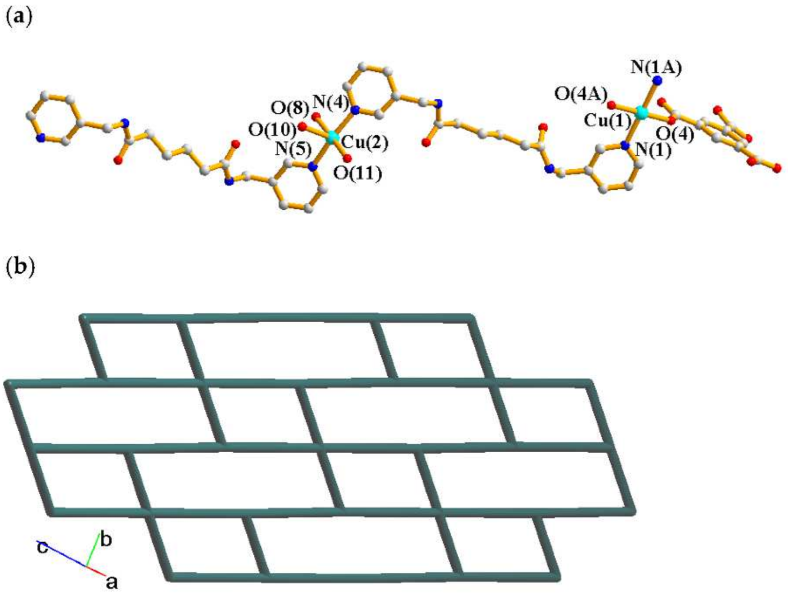

Figure 4. (**a**) Coordination environment of Cu(II) ions in **2**. Symmetry transformations used to generate equivalent atoms: (A) -x + 3, -y + 1, -z + 3. (**b**) A drawing showing the 2D net with the (4.6^2)$_2$(4^2.6^2.8^2)-**bex** topology.

2.3. Structure of **3**

Complex **3** crystallizes in the monoclinic space group *C*2/*c* and the asymmetric unit comprises one Cu(II) cation, a half of an **L**^{2} ligand and one 1,3,5-HBTB^{2-} ligand. The Cu(II) cation is coordinated by one nitrogen atom from the **L**^{2} ligand [Cu-N = 2.170(2) Å] and four oxygen atoms from four 1,3,5-HBTB^{2-} ligands [Cu-O = 1.9623(19) – 1.9763(18) Å], resulting in a distorted square pyramidal geometry, Figure 5a. Two Cu(II) cations are bridged by the 1,3,5-HBTB^{2-} ligand to form a dinuclear unit with a Cu---Cu distance of 2.6516(6) Å that is shorter than the sum of two van der Waals radius of Cu (2.8 Å), suggesting the presence of weak intermolecular forces. The Cu(II) ions are linked together by 1,3,5-HBTB^{2-} and **L**^{2} ligands to afford a 3D structure. If the dinuclear Cu(II) units are defined as 6-connected nodes, the structure can be simplified as a 6-connected net with the (4^{12}·6^3)-**pcu** topology, Figure 5b. The 3D nets penetrate into the neighbors to form a 3-fold 3D interpenetration structure, Figure 5c, demonstrating that the combination of the flexible **L**^{2} and 1,3,5-HBTB^{2-} may lead to the formation of the entangled CP [14].

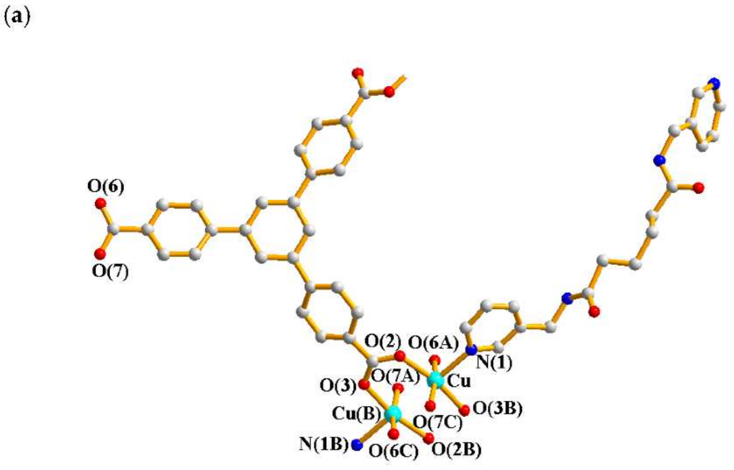

(**b**)

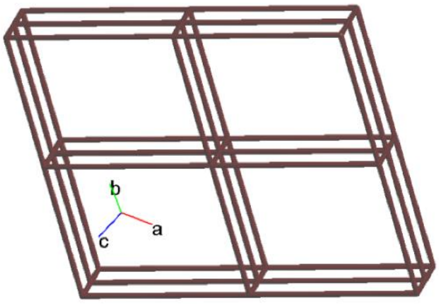

(**c**)

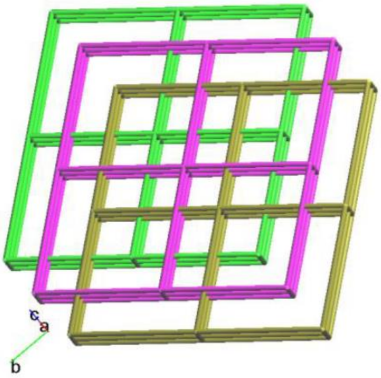

Figure 5. (a) Coordination environment of Cu(II) ions in **3**. Symmetry transformations used to generate equivalent atoms: (A) x + 1/2, -y + 1/2, z + 1/2; (B) -x + 1, -y + 1, -z + 2; (C) -x + 1/2, y + 1/2, -z + 3/2. (b) A drawing showing the structure with the **pcu** topology. (c) A drawing showing the 3-fold interpenetrated net.

2.4. Structure of **4**

Crystals of complex **4** conform to the monoclinic space group *C*2/*c*. The asymmetric unit consists of two Cu(II) cations, a half of an **L**^{3} ligand, one 1,3,5-BTC^{3-} ligand and one hydroxide ion. Figure 6a depicts the coordination environments about the Cu(II) ions. The Cu(1) and Cu(1B) atoms are symmetry-related by the inversion center and each atom is coordinated by one oxygen atom from the **L**^{3} ligand [Cu-O = 2.2720(16) Å], two oxygen atoms from two 1,3,5-BTC^{3-} ligands [Cu-O = 1.9377(14) - 19434(14) Å] and two oxygen atoms from two hydroxy groups [Cu-O = 1.9551(13) - 1.9620(13) Å], forming the square pyramidal geometry. On the other hand, each of the Cu(2) and Cu(2B) atoms is coordinated by one nitrogen atom from the **L**^{3} ligand [Cu-N = 2.0164(17) Å], three oxygen atoms from three 1,3,5-BTC^{3-} ligands [Cu-O = 1.9473(13) - 2.2909(15) Å] and one oxygen atom from the hydroxy group [Cu-O = 1.9482(13) Å], resulting in a distorted pentagonal bipyramidal geometry. The Cu(II) ions are linked together by 1,3,5-BTC^{3-} and **L**^{3} ligands to afford a 3D structure. If the tetranuclear Cu(II) units are defined as 10-connected nodes, 1,3,5-BTC^{3-} ligands as 3-connected nodes and **L**^{3} as 4-connected nodes, the structure can be simplified as a 3,4,10-connected trinodal net with the point symbol of $(4^{10}{\cdot}6^{32}{\cdot}8^3)(4^2{\cdot}6)_2(4^3{\cdot}6^3)$ topology, Figure 6b.

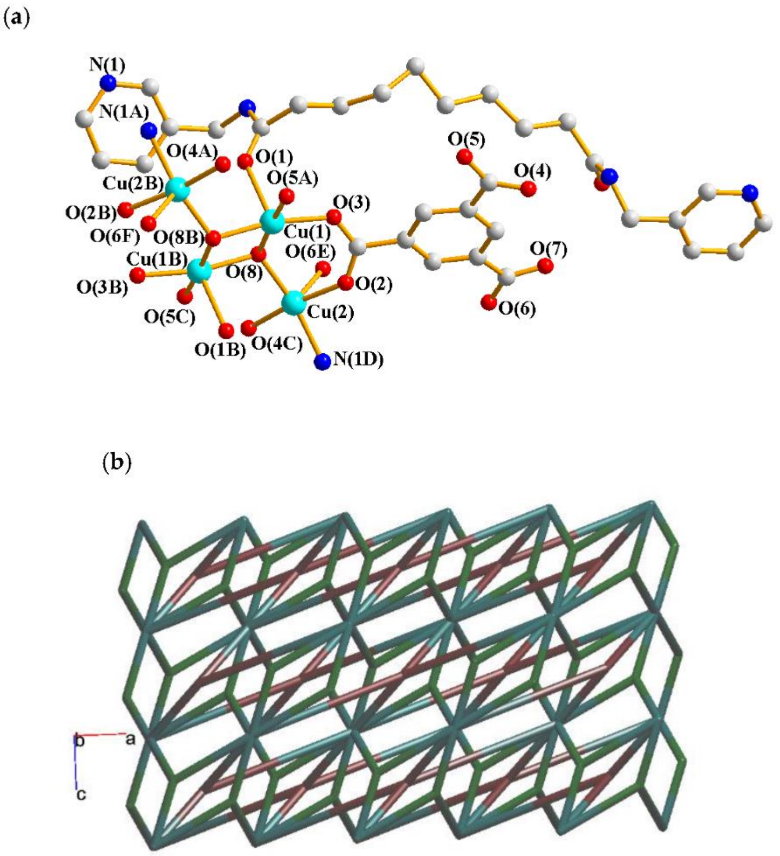

Figure 6. (**a**) Coordination environment of Cu(II) ions in **4**. Symmetry transformations used to generate equivalent atoms: (A) -x + 2, -y + 2, -z + 1; (B) -x + 3/2, -y + 3/2, -z + 1; (C) x - 1/2, y - 1/2, z; (D) x + 1/2, y - 1/2, z; (E) -x + 2, y, -z + 1/2; (F) x – 1/2, -y + 3/2, z + 1/2.). (**b**) A drawing showing the 3D framework with the $(4^{10}{\cdot}6^{32}{\cdot}8^{3})(4^{2}{\cdot}6)_{2}(4^{3}{\cdot}6^{3})$ topology.

2.5. Structure of **5** *and* **6**

Complexes **5** and **6** crystallize in the orthorhombic space group *P*na2₁. Each of the asymmetric units of **5** and **6** comprise three Cu(II) cations, two **L**³ ligands and two 1,3,5-BTB³⁻ ligands, with additional two and a half of a cocrystallized methanol molecule and two cocrystallized water molecules in **5**, and two cocrystallized DMF molecules and two cocrystallized water molecules in **6**, respectively. Figure 7a shows the coordination environments about the Cu(II) ions in **5**. While the Cu(1) atom is coordinated by one nitrogen atom from the **L**³ ligand [Cu(1)-N = 2.164(6) Å] and four oxygen atoms from four 1,3,5-BTB³⁻ ligands [Cu-O = 1.940(4) – 2.005(4) Å], the Cu(2) atom is coordinated by one nitrogen atom from **L**³ ligand [Cu(2)-N = 2.189(6) Å] and four oxygen atoms from four 1,3,5-BTB³⁻ ligands [Cu-O = 1.933(5) – 2.189(6) Å], resulting in square pyramidal geometries of both of the Cu(1) and Cu(2) atoms. The Cu(1) and Cu(2) atoms are bridged by the 1,3,5-BTB³⁻ ligands to form a dinuclear unit with a Cu---Cu distance of 2.6843(9) Å, indicating the presence of weak intermolecular forces. The Cu(3) atom is coordinated by two nitrogen atoms from two **L**³ ligand [Cu-N = 2.054(7) and 2.079(7) Å] and two oxygen atoms from two 1,3,5-BTB³⁻ ligands [Cu-O = 1.913(6) and 1.917(5) Å], displaying a distorted square planar geometry.

Figure 7b shows the coordination environments about the Cu(II) ions in **6**. The Cu(1) atom is coordinated by two nitrogen atoms from **L**³ ligand [Cu-N = 2.027(6) and 2.034(6) Å] and two oxygen atoms from two 1,3,5-BTB³⁻ ligands [Cu-O = 1.918(5) and 1.941(5) Å], resulting in a distorted square planar geometry. Each of the Cu(2) and Cu(3) atoms is coordinated by one nitrogen atom from **L**³ ligand [Cu(2)-N = 2.183(5) Å; Cu(3)-N = 2.181(6) Å] and four oxygen atoms from four 1,3,5-BTB³⁻ ligands [Cu(2)-O = 1.929(4) – 1.987(4) Å; Cu(3)-O = 1.929(4) – 2.016(4) Å], resulting in square pyramidal geometries for Cu(2) and Cu(3). The Cu---Cu distance of 2.6922(9) Å between Cu(2) and

Cu(3) is longer that in complex 5, indicating that the Cu(II)---Cu(II) interaction is subject to the nature of the cocrystallized solvent molecules. The Cu(II) ions in **5** and **6** are linked together by 1,3,5-BTB^{3-} and **L**^{3} ligands to afford 3D structures. If the dinuclear Cu(II) units are defined as 6-connected nodes, the mononuclear cations as 4-connected nodes and 1,3,5-BTB^{3-} as 3-connected nodes, while the **L**^{3} ligands as linkers, the structures of **5** and **6** can be simplified as 3,4,6-connected 3D nets with the point symbol of $(6^3)_2(6^4{\cdot}8^2)(6^8{\cdot}8^5{\cdot}10^2)$, Figure 7c.

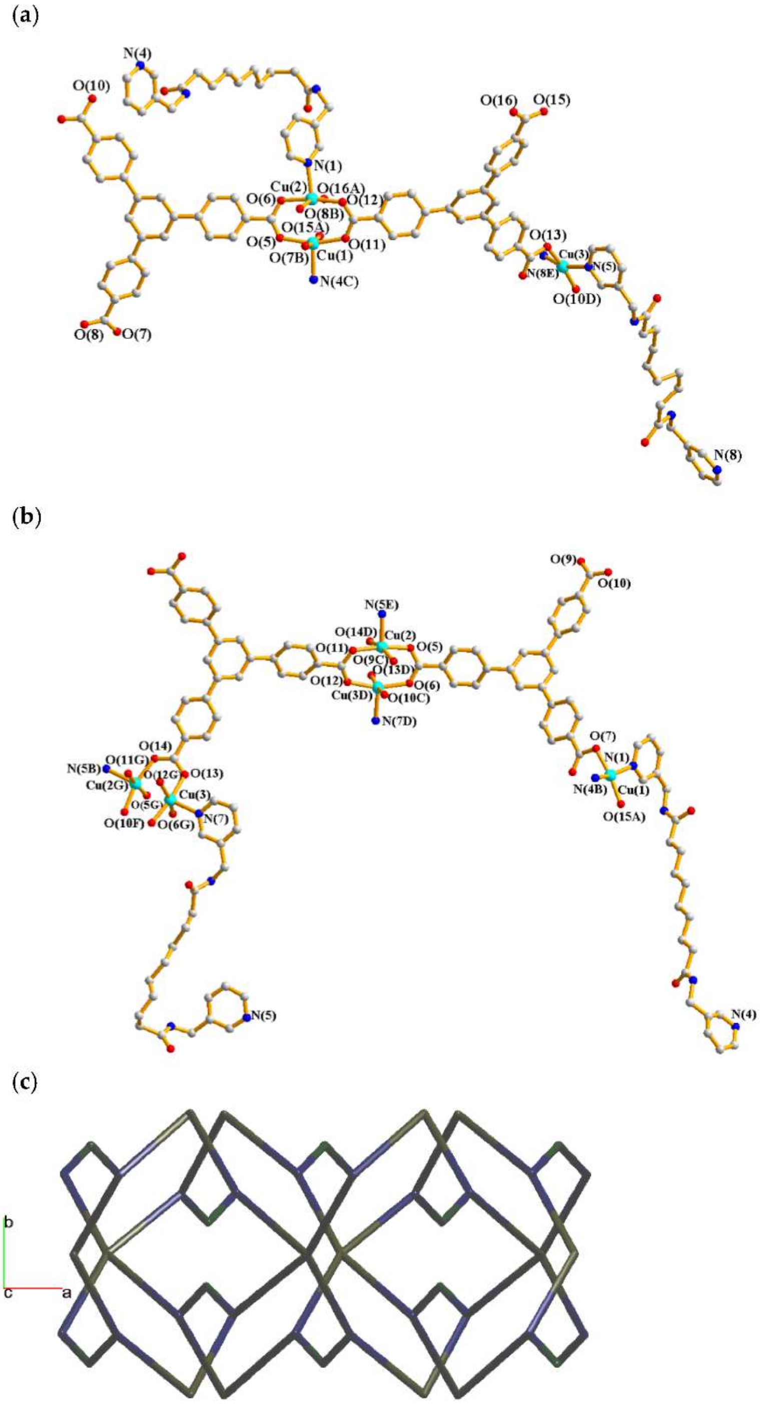

Figure 7. Coordination environments of Cu(II) ions in **5**. Symmetry transformations used to generate equivalent atoms: (A) x + 1/2, -y - 1/2, z; (B) x - 1/2, -y + 1/2, z; (C) x, y, z + 1; (D) -x + 1/2, y - 1/2, z + 3/2; (E) x, y, z – 1. (b) Coordination environment of Cu(II) ion in **6**. Symmetry transformations used to generate equivalent atoms: (A) -x + 5/2, y + 1/2, z + 3/2; (B) x, y, z – 1; (C) x - 1/2, -y + 3/2, z; (D) x + 1/2, -y + 1/2, z; (E) x + 1/2, -y + 1/2, z – 1; (F) x - 1, y - 1, z; (G) x - 1/2, -y + 1/2, z. (c) A drawing showing the 3,4,6-connected net with the point symbol $(6^3)_2(6^4{\cdot}8^2)(6^8{\cdot}8^5{\cdot}10^2)$.

2.6. Ligand Conformations and Coordination Modes

The ligand conformations of the bpba ligands have been proposed based on the torsion angles (θ) of their methylene carbon atoms [$0 \leq \theta \leq 90^o$, gauche (G) and $90 < \theta \leq 180^o$, anti (A)]. On the other hand, *cis* and *trans* are given if the two C=O groups are in the same and opposite directions, respectively. Three orientation, *syn-syn*, *syn-anti* and *anti-anti*, are also defined based on the relative position of pyridyl nitrogen and amide oxygen atoms [8]. Accordingly, the ligand conformations of **L^1** – **L^3** in **1** – **6** are listed in Table **1**. It is also noted that while the bpba ligands in **1**, **2**, **3**, **5** and **6** bridge two Cu(II) ions through the two pyridyl nitrogen atoms, that in **4** bridge four Cu(II) ions through two pyridyl nitrogen and two amide oxygen atoms. Noticeably, although complexes **5** and **6** adopt the same structural type, the ligand conformations of the **L^3** ligands are significantly different, presumably due to the difference in the cocrystallized solvents. Moreover, the tricarboxylate ligands in **1** – **6** bridge two to five Cu(II) ions through various coordination modes, which are also listed in Table 1.

Table 1. Ligand conformations and bonding modes of complexes **1** - **6**.

	Ligand conformation	Coordination mode
1	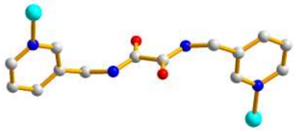 *trans syn-syn*	 μ_3-κO: κO′: κO″
2	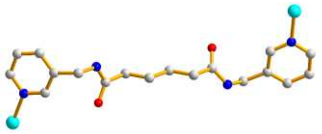 AAA *trans syn-syn*	 μ_2-κO:κO′
3	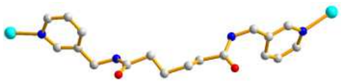 AGA *cis anti-anti*	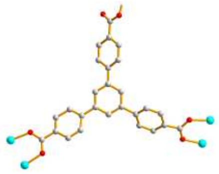 μ_4-κO: κO′: κO″: κO‴
4	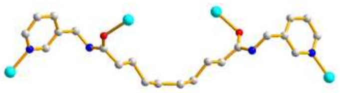 AAAAAAA *cis anti-anti*	 μ_5-κO:κO′:O″:O‴:O′′′′
5	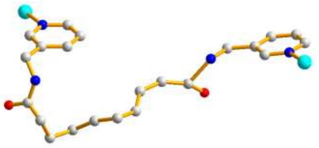 GGAAAAA *cis syn-syn*	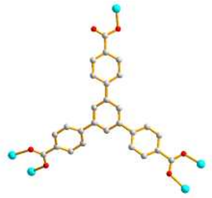 μ_5-κO:κO′:O″:O‴:O′′′′

6	 AAAAAAA *trans anti-anti*	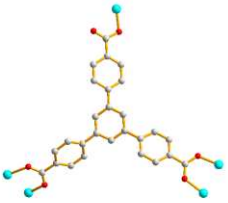 μ_5-κO:κO':O'':O''':O''''

2.7. Powder X-ray Analysis

In order to check the phase purity of the products, powder X-ray diffraction (PXRD) experiments have been carried out for all complexes. As shown in Figures S7–S12, the peak positions of the experimental and simulated PXRD patterns are in agreement with each other, which demonstrate that the crystal structures are truly representative of the bulk materials. The differences in intensity may be owing to the preferred orientation of the powder samples.

2.8. Thermal Properties

Thermal gravimetric analysis (TGA) was carried out to examine the thermal decomposition of 30 to 800 or 900 °C. The sample were heated in nitrogen gas at a pressure of 1 atm with heating rate of 10 °C min^{-1} and finished at 800 °C or 900 °C, Table 2, Figures S13–S18, indicating that complexes **1** – **6** display two-step weight loss involving loss of solvent and loss of organic ligands on heating.

Table 2. Thermal properties of complexes **1** - **6**.

Complex	Weight loss of solvent °C (calc/found), %	Weight loss of ligand °C (calc/found), %
1	H_2O 30 - 250 (3.21/4.38)	**L**^{1} + 1,3,5-HBTC^{2-} 250 - 800 (85.14/85.15)
2	6.5 H_2O 30 - 120 (16.19/14.38)	1.5 (**L**^{2}) + 1,3,5-BTC^{3-} 120 - 900 (73.64/70.97)
3	0.5 DMA + 3 H_2O 30 - 250 (12.83/7.86)	0.5 (**L**^{2}) + 1,3,5-HBTB^{2-} 250 - 800 (78.75/81.97)
4	-	**L**^{3} + 2 (1,3,5-BTC^{3-}) + 2 (OH$^-$) 270 - 800 (76.50/80.31)
5	2.5 MeOH + 2 H_2O 30 - 270 (5.97/4.28)	2 (**L**^{3}) + 2 (1,3,5-BTB^{3-}) 270 - 800 (84.12/85.60)
6	DMF + H_2O 30 - 250 (4.71/6.03)	2 (**L**^{3}) + 2 (1,3,5-BTB^{3-}) 250 - 800 (84.42/84.54)

2.9. Iodine Adsorption

Radioactive iodine such as ^{129}I represents one of the most critical nuclear wastes, which is harmful to human health and has to be captured and disposed of effectively. [15–17] On the other hand, CPs possessing porous structures may facilitate iodine adsorption through noncovalent interactions involving iodine and various sorption sites. Iodine adsorption experiments were thus carried out for complexes **1** - **6** to evaluate the degree of adsorption of iodine vapor at 25 and 60 °C within time interval of 30, 60, 120, 180 and 360 minutes, respectively. For each experiment, 10 mg of the complex was placed in a 4 mL sample bottle inside a 20 mL sample bottle containing 100 mg of iodine, which was then sealed and kept in the oven. Each experiment was repeated three times and the results averaged. It can be found that the colors of the complexes are different at different temperatures and time intervals, Figures S19–S30.

Tables S1–S12 summarize the I_2-adsorption of **1** - **6**, followed by the plots displaying iodine vapor adsorption rates. With the increase of temperature from 25 to 60 °C, the absorption rate of iodine also has a good increase for each complex, giving a best adsorption factor of 290.0 mg g^{-1} at 60 °C for 360 minutes for **5**. In order to confirm whether the structures of the iodine-adsorbed complexes remain unchanged, their powder X-ray diffraction (PXRD) patterns were measured. As shown in Figures S31–S42, most of the experimental patterns are consistent with the theoretical ones, but **2** at 60 °C for 30 and 60 minutes, and **5** and **6** at 60 °C for 60 minutes display some changes.

The ability of the CPs to adapt iodine molecules to the voids of the network structures may govern the iodine adsorption capacity [18–21]. The solvent accessible volumes calculated by using the PLATON program[22] for **1** – **6** were 1.5, 17.3, 34.4, 2.9, 11.8 and 10.4 %, respectively, of the unit cell volume, indicating that complex **3** that displays the 3-fold interpenetrated 3D net with the $(4^{12}{\cdot}6^{3})$-**pcu** topology may accommodate more iodine than the other complexes. However, the best adsorption factor of 290.0 mg g^{-1} at 60 °C for 360 minutes was observed for **5**, demonstrating the important role of the flexibility of the neutral spacer ligands, **L**^{1}, **L**^{2}, and **L**^{3}, in determining the iodine adsorption capacities of **1** – **6**. The 3D framework of **5** containing the flexible **L**^{3} may be more susceptible to the changes of the ligand conformation upon the attack of the iodine molecules and thus more appropriate to accommodate the iodine molecules, which can probably be verified by the subtle change of the PXRD pattern of **5**, Figure S40, upon iodine adsorption at 60 °C. On the other hand, the framework of the entangled **3** comprising **L**^{2} is not vulnerable to the iodine attack, thus allowing less iodine adsorption. The different performances in iodine adsorption between **5** and **6** are presumably due to the different cocrystallized solvents.

2.10. Energy Dispersive X-ray (EDX) Analysis

EDX analyses were performed for complexes **1** – **6** after iodine adsorption to investigate their iodine uptakes, Figures S43–S48. Three positions of the iodine-adsorbed sample of complexes 1 – 6 were selected for each measurement and the amount of iodine is different for each position, indicating the inhomogeneous distribution of iodine in the iodine-adsorbed sample.

2.11. Gas Adsorption

Low-pressure N_2 adsorption and desorption measurements were performed at 77 K for complexes **1** – **6**, which were heated at 120 °C for 24 hours to obtain fully activated samples before the measurements. Figures S49–S54 demonstrate that the complexes **1** and **3** – **6** remain stable upon the removal of the solvent molecules, while the structure of **2** has changed. The Brunauer–Emmet–Teller (BET) surface areas are 7.49, 13.60, 12.82, 12.60, 11.73, 7.98 m^2/g and the N_2 uptake capacities are 6.93, 18.33, 12.70, 11.28, 10.83 and 8.12 cm^3/g, respectively, for 1 – 6, Figures S55–S60, indicating larger surface area and N_2 uptake for **2** upon desolvation. Moreover, pore-size distribution curves show that the pore sizes are 2.9, 3.4, 3.4, 3.7, 3.4 and 3.4 nm respectively, for **1** – **6**, Figures S61–S66.

As demonstrated by the experiments, the BET surface area and N_2 uptakes of **1** – **6** derived from the low-pressure N_2 adsorption and desorption measurements are not closely related to their iodine adsorption capacities. Therefore, the iodine adsorption capacity may also depend on the characteristics of the CPs and their surface features.

3. Materials and Methods

3.1. Materials

The reagent $Cu(CH_3COO)_2{\cdot}H_2O$ was purchased from Showa, 1,3,5- benzenetricarboxylic acid (1,3,5-H_3BTC) from Alfa Aesar and 1,3,5-tri(4-carboxyphenyl)benzene (1,3,5-H_3BTB) from Alfa Aesar. The ligands *N,N′*-bis(3-methylpyridyl)oxalamide (**L**^{1}), *N,N′*-bis(3-methylpyridyl)adipoamide (**L**^{2})

and *N,N′*-bis(3-methylpyridyl)sebacoamide (**L**^{3}) were prepared according to published procedures [23–25].

3.2. Preparations

3.3.1.{[. Cu(**L**^{1})(1,3,5-HBTC)]·H_2O}$_n$, **1**

A mixture of $Cu(CH_3COO)_2\cdot H_2O$ (0.020 g, 0.10 mmol), **L**^{1} (0.027 g, 0.10 mmol) and 1,3,5-H_3BTC (0.021 g, 0.10 mmol) in 10 mL of H_2O was sealed in a 23 mL Teflon-lined steel autoclave, which was heated under autogenous pressure to 120 °C for two days, and then cooled down to room temperature for two days. Blue crystals suitable for single-crystal X-ray diffraction were obtained. Yield: 0.081 g (72 %). Anal. Calcd for $C_{23}H_{20}CuN_4O_9$ (MW = 599.97): C, 49.33; N, 10.00; H, 3.60 %. Found: C, 49.39; N, 9.85; H, 3.48 %. FT-IR (cm^{-1}): 3313(s), 2357(m), 1621(s), 1519(m), 1430(m), 1351(s), 1099(m), 860(w), 756(m), 609(w), 512(w).

3.2.2.{[. $Cu_{1.5}$(**L**^{2})$_{1.5}$(1,3,5-BTC)(H_2O)$_2$]·6.5H_2O}$_n$, **2**

Complex **2** was prepared by following the similar procedures for **1**, except that $Cu(CH_3COO)_2\cdot H_2O$ (0.020 g, 0.10 mmol), **L**^{2} (0.033 g, 0.10 mmol) and 1,3,5-H_3BTC (0.021 g, 0.10 mmol) in 10 mL of NaOH (0.01 M) aqueous solution were used, which was heated at 100 °C. Blue crystals were obtained. Yield: 0.054 g (86 %). Anal. Calcd for $C_{36}H_{53}Cu_{1.5}N_6O_{17.50}$ (MW = 945.15): C, 45.75; N, 8.89; H, 5.65 %. Found: C, 46.19; N, 8.69; H, 5.62 %. FT-IR (cm^{-1}): 3054(m), 2359(m), 1606(s), 1427(m), 1352(s), 1196(m), 1058(w), 811(w), 710 (m).

3.3.3.[. Cu(**L**^{2})$_{0.5}$(1,3,5-HBTB)]$_n$, 3

Complex **3** was prepared by following the similar procedures for **1**, except that $Cu(CH_3COO)_2\cdot H_2O$ (0.020 g, 0.10 mmol), **L**^{2} (0.033 g, 0.10 mmol) and 1,3,5-H_3BTB (0.044 g, 0.10 mmol) in 7 mL of H_2O and 3 mL of DMA were used. Green crystals were obtained. Yield: 0.032 g (42 %). Anal Calcd for $C_{36}H_{27}CuN_2O_7$ (MW = 663.13): C, 65.20; N, 4.22; H, 4.10 %. Anal Calcd for $C_{36}H_{27}CuN_2O_7\cdot 0.5DMA\cdot 3H_2O$ (MW = 760.72): C, 59.99; N, 4.60; H, 4.97 %. Found: C, 59.94; N, 4.84; H, 4.73 %. FT-IR (cm^{-1}): 2360(m), 1604(s), 1390(s), 1176(w), 1015(m), 853(w), 774(s), 669(w).

3.3.4.[. Cu_4(**L**^{3})(OH)$_2$(1,3,5-BTC)$_2$]$_n$, **4**

Complex **4** was prepared by following the similar procedures for **1**, except that $Cu(CH_3COO)_2\cdot H_2O$ (0.020 g, 0.10 mmol), **L**^{3} (0.038 g, 0.10 mmol) and 1,3,5-H_3BTC (0.021 g, 0.10 mmol) in 10 mL of H_2O were used. Blue crystals were obtained. Yield: 0.016 g (60 %). Anal. Calcd for $C_{40}H_{38}Cu_4N_4O_{16}$ (MW = 1084.90): C, 44.28; N, 5.16; H, 3.53 %. Found: C, 44.49; N, 5.22; H, 3.87 %. FT-IR (cm^{-1}): 3238 (m), 2363(m), 1583(s), 1442(m), 1353(s),1094(w), 761(m), 716(m), 586(w).

3.3.5.{[. Cu_3(**L**^{3})$_2$(1,3,5-BTB)$_2$]·2.5MeOH·2H_2O}$_n$, **5**, and {[Cu_3(**L**^{3})$_2$(1,3,5-BTB)$_2$]·DMF·2H_2O}$_n$, **6**

Complexes **5** and **6** were prepared by following the similar procedures for **1**, but in different solvent systems. While complex **5** was prepared from a reaction mixture of $Cu(CH_3COO)_2\cdot H_2O$ (0.020 g, 0.10 mmol), **L**^{3} (0.038 g, 0.10 mmol) and 1,3,5-H_3BTB (0.044 g, 0.10 mmol) in 3 mL of H_2O and 7 mL of MeOH, complex **6** was obtained in 7 mL of H_2O and 3 mL of DMF. Green crystals were obtained for **5**. Yield: 0.018 g (28 %). Anal. Calcd for $C_{100.50}H_{104}Cu_3N_8O_{20.50}$ (MW = 1942.53): C, 62.14; N, 5.77; H, 5.40 %. Found: C, 61.93; N, 5.59; H, 4.86 %. FT-IR (cm^{-1}): 3068(m), 2925(m), 2360(w), 1596(s), 1406(s), 1179(w), 1015(w), 854(w), 778(m), 700(w). Green crystals were obtained for **6**. Yield: 0.036 g (56 %). Anal. Calcd for $C_{101}H_{101}Cu_3N_9O_{19}$ (MW = 1935.52): C, 62.67; N, 6.51; H, 5.26 %. Anal. Calcd for **6** + 3 H_2O, $C_{101}H_{107}Cu_3N_9O_{22}$ (MW = 1989.52): C, 60.97; N, 6.34; H, 5.42 %. Found: C, 60.67; N, 6.33; H, 5.02 %. FT-IR (cm^{-1}): 3065(m), 2357(w), 1599(s), 1393(s), 1177(w), 1015(m), 851(m), 775(s), 702(m), 668(w).

The IR spectra of complexes **1** – **6** are provided as Figures S1–S6 in the Supplementary Materials.

Preprints (www.preprints.org) | NOT PEER-REVIEWED | Posted: 5 December 2023 doi:10.20944/preprints202312.0220.v1

3.5. X-ray Crystallography

A Bruker AXS SMART APEX II CCD diffractometer, equipped with a graphite-monochromated MoK*α* radiation (0.71073 Å), was used to collect diffraction data for complexes **1** – **6**. The diffraction data were then reduced by using standard methods [26], followed by empirical absorption corrections based on "multi-scan". The positions of some of the heavier atoms were located by direct method or Patterson method and the remaining atoms were found in a series of alternating difference Fourier maps and least-square refinements. The hydrogen atoms except those of the water molecules were added by using the HADD command in SHELXTL 6.1012 [27] Due to the serious disordering, the solvent molecules in **3** were squeezed by using the PLATON program [22] and their diffraction data were reported without solvent contribution. Table 3 lists the crystal and structure refinement parameters for **1** – **6**. CCDC no. 2311169-2311174 contain the supplementary crystallographic data for this paper. These data can be obtained free of charge via http://www.ccdc.cam.ac.uk/conts/retrieving.html or from the Cambridge Crystallographic Data Centre, 12 Union Road, Cambridge CB2 1EZ, UK; fax: +44 1223 336 033; e-mail: deposit@ccdc.cam.ac.uk; or at www: http://www.ccdc.cam.ac.uk .

Table 3. Crystal data for complexes **1** - **6.**

Complex	**1**	**2**	**3**
Formula	$C_{23}H_{20}CuN_4O_9$	$C_{36}H_{53}Cu_{1.5}N_6O_{17.50}$	$C_{36}H_{27}CuN_2O_7$
Formula weight	599.97	945.15	663.13
Crystal system	Triclinic	Triclinic	Monoclinic
Space group	$P\bar{1}$	$P\bar{1}$	$C2/c$
a, Å	10.1482(9)	8.9062(2)	18.8531(6)
b, Å	11.1855(10)	11.2565(3)	25.8032(8)
c, Å	11.7055(11)	22.7418(5)	17.4503(6)
α, °	111.285(3)	99.7718(14)	90
β, °	97.429(3)	94.3827(15)	99.4362(19)
γ,°	108.425(3)	105.8728(14)	90
V, $Å^3$	1128.97(18)	2142.95(9)	8374.2(5)
Z	2	2	8
D_{calc}, Mg/m^3	1.647	1.465	1.052
F(000)	574	989	2736
μ(Mo $K_α$), mm^{-1}	1.032	0.831	0.561
Range(2θ) for data collection, deg	$3.88 \le 2θ \le 51.99$	$3.66 \le 2θ \le 56.62$	$3.34 \le 2θ \le 56.62$
Independent reflection	4415	10315	10067
	[R(Int) = 0.0643]	[R(Int) = 0.0539]	[R(Int) = 0.0745]
Data / restraint / parameter	4415 / 0 / 338	10315 / 0 / 556	10067 / 0 / 432
quality-of-fit indicator^c	1.054	1.015	0.990
Final R indices	$R_1 = 0.0555$,	$R_1 = 0.0550$,	$R_1 = 0.0536$,
$[I > 2σ(I)]$ ^{a,b}	$wR_2 = 0.1419$	$wR_2 = 0.1228$	$wR_2 = 0.1164$
R indices (all data)	$R_1 = 0.0755$,	$R_1 = 0.1158$,	$R_1 = 0.1022$,
	$wR_2 = 0.1668$	$wR_2 = 0.1452$	$wR_2 = 0.1345$
Formula	$C_{40}H_{38}Cu_4N_4O_{16}$	$C_{100.50}H_{104}Cu_3N_8O_{20.50}$	$C_{101}H_{101}Cu_3N_9O_{19}$
Formula weight	1084.90	1942.53	1935.52
Crystal system	Monoclinic	Orthorhombic	Orthorhombic
Space group	$C2/c$	$Pna2_1$	$Pna2_1$
a, Å	16.5969(9)	20.9682(10)	22.0739(18)
b, Å	13.9067(4)	25.3489(11)	24.3392(18)
c, Å	17.6110(5)	18.1699(8)	17.9481(15)
α, °	90	90	90
β, °	90.2248(9)	90	90
γ,°	90	90	90

V, Å^3	4064.73(19)	9657.7(8)	9642.8(13)
Z	4	4	4
D_{calc}, Mg/m^3	1.773	1.336	1.333
F(000)	2200	4056	4036
μ(Mo K_α), mm^{-1}	2.145	0.728	0.728
Range (2θ) for data collection,deg	$3.82 \le 2\theta \le 56.59$	$2.75 \le 2\theta \le 51.99$	$2.82 \le 2\theta \le 56.63$
Independent reflection	5049 [R(Int) = 0.0283]	18994 [R(Int) = 0.0510]	20288 [R(Int) = 0.0765]
Data / restraint / parameter	5049 / 0 / 311	18994 / 2119 / 1157	20288 / 1 / 1181
quality-of-fit indicator^c	1.085	1.026	1.002
Final R indices [I > 2σ(I)] ^{a,b}	R_1 = 0.0265, wR_2 = 0.0690	R_1 = 0.0526, wR_2 = 0.1408	R_1 = 0.0571, wR_2 = 0.1019
R indices (all data)	R_1 = 0.0323, wR_2 = 0.0747	R_1 = 0.0664, wR_2 = 0.1503	R_1 = 0.1364, wR_2 = 0.1244

$^{a}R_1 = \Sigma||F_o| - |F_c|| / \Sigma|F_o|$. $^{b}wR_2 = [\Sigma w(F_o^2 - F_c^2)^2 / \Sigma w(F_o^2)^2]^{1/2}$. $w = 1 / [\sigma^2(F_o^2) + (ap)^2 + (bp)]$, $p = [\max(F_o^2 \text{ or } 0) + 2(F_c^2)] / 3$. a = 0.1039, b = 1.1215 for 1; a = 0.0650, b = 0 for 2; a = 0.0585, b = 0 for 3; a = 0.0330, b = 9.2346 for 4; a = 0.0856, b = 10.2363 for 5; a = 0.0496, b = 0 for 6. ^{c}quality-of-fit = $[\Sigma w(|F_o^2| - |F_c^2|)^2 / N_{observed} - N_{parameters})]^{1/2}$.

4. Conclusions

Six new CPs supported by the mixed ligands with different flexibility have been synthesized. Complexes **1** – **4** form a 2D layer with the {$4^4.6^2$}-sql topology, a 2D layer with the $(4.6^2)_2(4^2.6^2.8^2)$-**bex** topology, a 3-fold interpenetrated 3D net with the $(4^{12}\cdot 6^3)$-**pcu** topology and a 3D net with the $(4^{10}\cdot 6^{32}\cdot 8^3)(4^2\cdot 6)_2(4^3\cdot 6^3)$ topology, respectively, whereas **5** and **6** are 3D nets with the same $(6^3)_2(6^4\cdot 8^2)(6^8\cdot 8^5\cdot 10^2)$ topology, showing that the use of the extended 1,3,5-H_3BTB afforded different structural types as compared with those derived from 1,3,5-H_3BTC and combination of the flexible $\mathbf{L^2}$ with 1,3,5-H_3BTB gave an entangled CP. Among the six CPs, complex **5** reveals the best iodine-adsorption capacity. This report offers an insight into understanding the roles of the flexibility of the bpba and tricarboxylate ligands in determining the structural diversity as well as the iodine adsorption capacity.

Supplementary Materials: The following supporting information can be downloaded at the website of this paper posted on Preprints.org.

Author Contributions: Investigation, S.-Y.L.; data curation, Y.-L.S. and W.-H.C.; review and supervision, M.G. and J.-D.C. All authors have read and agreed to the published version of the manuscript.

Funding: This research was funded by the National Science and Technology Council of the Republic of China: NSTC 112-2113-M-033-004.

Institutional Review Board Statement: Not applicable.

Informed Consent Statement: Not applicable.

Data Availability Statement: Data are contained within the article or Supplementary Material.

Acknowledgments: We are grateful to the National Science and Technology Council of the Republic of China for support.

Conflicts of Interest: The authors declare no conflict of interest.

References

1. Tiekink, E.R.; Vittal, J.J. Frontiers in Crystal Engineering. **2006**.
2. Batten, S.R.; Neville, S.M.; Turner, D.R. Coordination Polymers Design, Analysis and Application; The Royal Society of Chemistry: London, **2009**.
3. Allendorf, M.D.; Bauer, C.A.; Bhakta, R.K.; Houk, R.J.T. Luminescent metal–organic frameworks. *Chem. Soc. Rev.* **2009**, *38*, 1330.

4. Shi, Y.X.; Zhang, W.H.; Abrahams, B.F.; Braunstein, P.; Lang, J.P. Fabrication of Photoactuators: Macroscopic Photomechanical Responses of Metal-Organic Frameworks to Irradiation by UV Light. *Angew. Chem. Int. Ed.* **2019**, *58*, 9453−9458.
5. Shi, Y.X.; Chen, H.H.; Zhang, W.H.; Day, G.S.; Lang, J.P.; Zhou, H.C. Photoinduced nonlinear contraction behavior in metalorganic frameworks. *Chem. Eur. J.* **2019**, *25*, 8543−8549.
6. Liu, D.; Lang, J.-P.; Abrahams, B.F. Highly Efficient Separation of a Solid Mixture of Naphthalene and Anthracene by a Reusable Porous Metal−Organic Framework through a Single-Crystal-to-Single Crystal Transformation. *J. Am. Chem. Soc.* **2011**, *133*, 11042.
7. Liu, C.-Y.; Chen, X.-R.; Chen, H.-X.; Niu, Z.; Hirao, H.; Braunstein, P.; Lang, J.-P. Ultrafast Luminescent Light-Up Guest Detection Based on the Lock of the Host Molecular Vibration. *J. Am. Chem. Soc.* **2020**, *142*, 6690−6697.
8. Kedar, B.T.; Chen, J.-D. Crystal engineering of coordination polymers containing flexible bis-pyridyl-bis-amide ligands. *CrystEngComm*. **2015**, *17*, 4611–4626.
9. Mondal, S.; Dastidar, P. Mixed Ligand Coordination Polymers for Metallogelation and Iodine Adsorption. *Cryst. Growth Des.* **2019**, *19*, 470−478.
10. Chen, C.-J.; Chen, C.-L.; Lee, W.-T.; Hu, J.-H.; Chhetri, P.M.; Chen, J.-D., Coordination polymers with a semi-rigid spacer ligand in a mixed system: Roles of benzene-1, 3, 5-tricarboxylate anions. *J. Mol. Struct.* **2021**, *1244*, 131252.
11. Hu, J.H.; Liu, Y.C.; Chen, J.-D. Cobalt (II) coordination polymers constructed from bis (N-pyrid-3-ylmethyl) adipoamide and polycarboxylic acids: Reversible structural transformation upon proton delivery and removal. *CrystEngComm* **2021**, *23*, 7471-7478.
12. Hu, J.H.; Liu, Y.C.; Liu, Y.H.; Chen, J.-D. Structural transformations in cobalt (ii) coordination polymers constructed from flexible N, N′-bis (3-pyridylmethyl) sebacoamide and benzene-1, 3, 5-tricarboxylic acid. *CrystEngComm* **2022**, *24*, 4120-4127.
13. Blatov, V.A.; Shevchenko, A.P.; Proserpio, D.M. Applied topological analysis of crystal structures with the program package ToposPro. *Cryst. Growth Des.* **2014**, *14*, 3576-3586.
14. Huang, W.-C.; Chen, W.-H.; Chen, C.-L.; Liao, T.-T.; Chen, Y.-W.; Chen, J.-D. Formation of entangled Co(II) coordination polymers based on bis-pyridyl-bis-amide and angular dicarboxylate ligands: A structural comparison. *CrystEngComm* **2023**, *25*, 5575–5587.
15. Safarifard, V.; Morsali, A. Influence of an amine group on the highly efficient reversible adsorption of iodine in two novel isoreticular interpenetrated pillared-layer microporous metal–organic frameworks. *CrystEngComm*. **2014**, *16*, 8660-8663.
16. Guo, B.; Li, F.; Wang, C.; Zhang, L.; Sun, D. A rare (3, 12)-connected zirconium metal–organic framework with efficient iodine adsorption capacity and pH sensing. *J. Mater. Chem. A.* **2019**, *7*, 13173–13179.
17. Arici, M.; Arici, T.A.; Demiral, H., Taş, M.; Yeşilel, O.Z. A porous Zn (II)-coordination polymer based on a tetracarboxylic acid exhibiting selective CO 2 adsorption and iodine uptake. *Dalton Trans.* **2020**, *49*, 10824-10831.
18. Lee, W.T.; Liao, T.T.; Chen, J.-D. Nickel (II) Coordination Polymers Supported by Bis-pyridyl-bis-amide and Angular Dicarboxylate Ligands: Role of Ligand Flexibility in Iodine Adsorption. *Int. J. Mol. Sci.* **2022**, *23*, 3603.
19. Mohanambe, L.; Vasudevan, S. Insertion of iodine in a functionalized inorganic layered solid. *Inorg. Chem.* **2004**, *43*, 6421-6425.
20. Zhang, N.; Sun, L.X.; Bai, F.Y.; Xing, Y.H. Thorium–organic framework constructed with a semirigid triazine hexacarboxylic acid ligand: Unique structure with thorium oxide wheel clusters and iodine adsorption behavior. *Inorg. Chem.* **2020**, *59*, 3964–3973.
21. Liu, J.H.; Qi, Y.J.; Zhao, D.; Li, H.H.; Zheng, S.T. Heterometallic organic frameworks built from trinuclear indium and cuprous halide clusters: Ligand-oriented assemblies and iodine adsorption behavior. *Inorg. Chem.* **2018**, *58*, 516-523.
22. Spek, A.L. checkCIF validation ALERTS: What they mean and how to respond. *Acta Crystallogr.* **2020**, *E76*, 1-11.
23. Liu, Y.F.; Hu, J.H.; Lee, W.T.; Yang, X.K.; Chen, J.-D. Structural transformations of cobalt (II) coordination polymers constructed from N, N′-di-3-pyridyladipoamide and tetracarboxylic acids: Disentanglement upon water coordination. *Cryst. Growth Des.* **2020**, *20*, 7211-7218.

24. Liao, T.-T.; Lin, S.-Y.; Chen, J.-D. Co (ii) coordination polymers supported by a benzenetetracarboxylate and bis-pyridyl-bis-amides with different flexibilities. *CrystEngComm* **2023**, *25*, 1723–1730.
25. Liu, Y.-H.; Liao, T.-T.; Lin, S.-Y.; Zhong, S.-Y.; Chen, T.-R.; Chen, J.-D. Cd (II) and Zn (II) coordination polymers constructed from bis-pyridyl-bis-amide and dicarboxylic or tetracarboxylic acid: Synthesis, structures and luminescent properties. *Inorg. Chim. Acta.* **2023**, *556*, 121641.
26. Bruker AXS. APEX2, V2008.6, SADABS V2008/1, SAINT V7.60A, SHELXTL V6.14; Bruker AXS Inc.: Madison, WI, USA, **2008**.
27. Sheldrick, G.M. Crystal structure refinement with SHELXL. *Acta Crystallogr.* **2015**, *C71*, 3-8.